Project Report
ATC-322

Extended-Range Signal Recovery Using Multi-PRI Transmission for Doppler Weather Radars

J.Y.N. Cho

1 November 2005

Lincoln Laboratory
MASSACHUSETTS INSTITUTE OF TECHNOLOGY
LEXINGTON, MASSACHUSETTS

Prepared for the Federal Aviation Administration,
Washington, D.C. 20591

TECHNICAL REPORT STANDARD TITLE PAGE

1. Report No.	2. Government Accession No.	3. Recipient's Catalog No.
ATC-322		

4. Title and Subtitle	5. Report Date
Extended-Range Signal Recovery Using Multi-PRI Transmission for Doppler Weather Radars	1 November 2005
	6. Performing Organization Code

7. Author(s)	8. Performing Organization Report No.
John Y.N. Cho	ATC-322

9. Performing Organization Name and Address	10. Work Unit No. (TRAIS)
MIT Lincoln Laboratory 244 Wood Street Lexington, MA 02420-9108	11. Contract or Grant No. FA8721-05-C-0002

12. Sponsoring Agency Name and Address	13. Type of Report and Period Covered
Department of Transportation Federal Aviation Administration 800 Independence Ave., S.W. Washington, DC 20591	Project Report
	14. Sponsoring Agency Code

15. Supplementary Notes

This report is based on studies performed at Lincoln Laboratory, a center for research operated by Massachusetts Institute of Technology, under Air Force Contract FA8721-05-C-0002.

16. Abstract

Range-velocity (RV) ambiguity is a source of data quality degradation common to all weather radars. Various methods have been developed in recent years to combat this problem. For example, for the new NEXRAD Open Radar Data Acquisition (ORDA) system, the primary focus for range-overlay separation has been on phase-code transmission and processing techniques. There are, however, conditions under which the phase-code method fails to separate range-overlaid signals, e.g., when the overlaid power ratio is too high or the Doppler spectra are too wide. Phase-code processing also has no intrinsic capacity for velocity dealiasing.

To address these issues, Lincoln Laboratory developed an alternative RV ambiguity mitigation scheme using multiple pulse-repetition interval (multi-PRI) transmission and processing. The range-dealiasing performance of the multi-PRI approach complements the capability of the phase-code technique. It can succeed when phase-code processing fails, and where it fails, phase-code processing succeeds (e.g., when an overlaid patch of signal is continuous and extensive in the radial direction). Multi-PRI also provides velocity dealiasing.

However, because the multi-PRI algorithm was constructed for the Terminal Doppler Weather Radar (TDWR) with its primary mission of short-range coverage around airports, only the capability of first-trip protection was explicitly developed. This report extends the multi-PRI technique to the recovery of Doppler data from other trips, out to the long-range surveillance limit of NEXRAD. Simulated and real weather radar data are used to demonstrate the capabilities and limitations of the technique.

17. Key Words	18. Distribution Statement
Range-velocity, multi-PRI, phase-code technique, velocity dealiasing	This document is available to the public through the National Technical Information Service, Springfield, VA 22161.

19. Security Classif. (of this report)	20. Security Classif. (of this page)	21. No. of Pages	22. Price
Unclassified	Unclassified	30	

EXECUTIVE SUMMARY

Range-velocity (RV) ambiguity is a source of data quality degradation common to all weather radars. Various methods have been developed in recent years to combat this problem. For example, for the new NEXRAD Open Radar Data Acquisition (ORDA) system, the primary focus for range-overlay separation has been on phase-code transmission and processing techniques. There are, however, conditions under which the phase-code method fails to separate range-overlaid signals, e.g., when the overlaid power ratio is too high or the Doppler spectra are too wide. Phase-code processing also has no intrinsic capacity for velocity dealiasing.

To address these issues, Lincoln Laboratory developed an alternative RV ambiguity mitigation scheme using multiple pulse-repetition interval (multi-PRI) transmission and processing. The range-dealiasing performance of the multi-PRI approach complements the capability of the phase-code technique. It can succeed when phase-code processing fails, and where it fails, phase-code processing succeeds (e.g., when an overlaid patch of signal is continuous and extensive in the radial direction). Multi-PRI also provides velocity dealiasing.

However, because the multi-PRI algorithm was constructed for the Terminal Doppler Weather Radar (TDWR) with its primary mission of short-range coverage around airports, only the capability of first-trip protection was explicitly developed. This report extends the multi-PRI technique to the recovery of Doppler data from other trips, out to the long-range surveillance limit of NEXRAD. Simulated and real weather radar data are used to demonstrate the capabilities and limitations of the technique.

TABLE OF CONTENTS

		Page
	EXECUTIVE SUMMARY	iii
	List of Illustrations	vii
1.	INTRODUCTION	1
2.	RANGE DEALIASING	3
3.	RESULTS USING SIMULATED WEATHER RADAR DATA	7
4.	RESULTS USING REAL WEATHER RADAR DATA	13
5.	SUMMARY DISCUSSION	17
	Glossary	19
	References	21

LIST OF ILLUSTRATIONS

Figure No.		Page
1	Illustration of how an out-of-trip signal can be separated from the first-trip signal by transmitting at more than one PRI.	3
2	Reflectivity field input to simulated weather radar data.	8
3	SNR field input to simulated weather radar data.	9
4	Radial velocity field input to simulated weather radar data.	9
5	Reflectivity estimated from processed MBS signal.	10
6	Radial velocity estimated from processed MBS signal.	11
7	Spectral width estimated from processed MBS signal.	11
8	Reflectivity estimates from a long-PRI (3.06 ms) scan.	14
9	Reflectivity estimates from the MBS transmitted signal with range dealiasing.	14
10	Radial velocity estimates from the MBS transmitted signal with range dealiasing.	15
11	Spectral width estimates from the MBS transmitted signal with range dealiasing.	15

1. INTRODUCTION

The unambiguous range, r_a, and velocity, v_a, of Doppler radars are constrained by the relation $r_a v_a = c\lambda/8$, where c is the speed of light and λ is the wavelength. In terms of the pulse repetition interval (PRI), $r_a = cT/2$ and $v_a = \lambda/(4T)$, where T is the PRI value. For example, a 10-cm-wavelength weather radar (such as the Weather Surveillance Radar-1988 Doppler (WSR-88D)) with PRI set for $r_a = 230$ km would have a v_a of only 16 m s^{-1}. The constraint is even more severe for shorter wavelength radars. Thus, the long-range surveillance requirement for ground-based weather radars is not compatible with the need to measure the full range of wind velocities in the troposphere without the application of techniques to work around this range-velocity (RV) conundrum.

There are existing methods such as phase-code (e.g., Siggia 1983; Sachidananda and Zrnić 1999) and staggered PRI (e.g., Sachidananda and Zrnić 2002) processing that exploit diversity in pulse phase and timing to combat RV ambiguity. In a previous paper we proposed an alternative multi-PRI approach to RV ambiguity mitigation (Cho 2005). That paper, however, was focused on application to the Terminal Doppler Weather Radar (TDWR), and, thus, only discussed methods for protecting first-trip signals from range overlays. (The primary mission of the TDWR is wind-shear detection in the vicinity of the airport, with a velocity measurement requirement to only 89 km.) In this paper we will extend the results to include range-dealiased estimates of reflectivity, radial velocity, and spectral width from all trips, with an eye toward application to the WSR-88D.

2. RANGE DEALIASING

The principle behind range dealiasing using multi-PRI transmission is straightforward. Suppose we are interested in obtaining base data estimates at range r_t, which is in the second-trip range of PRI #1 with corresponding unambiguous range r_{a1}. The signal returned from r_t would then be overlaid on the first-trip gate at $r_t - r_{a1}$ (Figure 1, top). If no other PRIs are used within the dwell, then all pulse returns from r_t would be sampled at $r_t - r_{a1}$. Furthermore, if the signal from the first trip is much greater than the signal from r_t, then the second-trip information cannot be extracted except through phase-code processing. However, if other PRIs are used within the dwell, then the signal from target range r_t will be overlaid on other first-trip gates, e.g., for PRI #2 the corresponding first-trip gate would be $r_t - r_{a2}$ (Figure 1, bottom). Now there is the possibility that the signal from these other first-trip ranges will be less than the signal from r_t. If so, then the data from those first-trip gates can be used to recover the information from r_t.

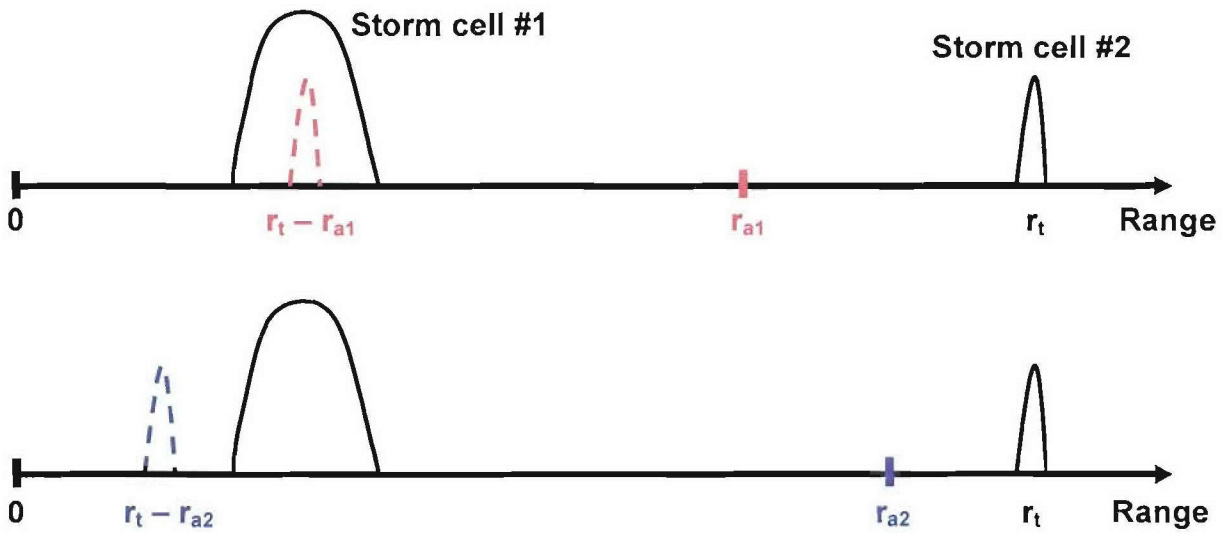

Figure 1. Illustration of how an out-of-trip signal can be separated from the first-trip signal by transmitting at more than one PRI. The diagram shows two storm cells, one near and the other far. If only one PRI is used, signal from the far cell aliases into the same range as the nearby cell (top). In this case, the second-trip signal is overwhelmed by the first-trip signal. A different PRI causes the far cell to alias to a range away from the nearby cell (bottom). Since there is no significant first-trip signal, the second-trip signal can be recovered.

Why not just use a constant PRI and apply phase-code processing? It turns out that phase-code and multi-PRI processing have complementary capabilities (Cho et al. 2003). The multi-PRI technique is impervious to overlays with strong signals or wide spectral widths, whereas phase-code methods fail to separate the different trip signals under such conditions. When the unwanted overlaid signal continuously spans a long radial distance, however, the multi-PRI approach fails, whereas the phase-code techniques are unaffected. This observation led us to propose an adaptive scheme for the upgraded TDWR radar data acquisition (RDA) system, whereby information from an initial long-PRI scan would be used to select multi-PRI or phase-code signal transmission and processing on a radial-by-radial basis in the subsequent scan (Cho 2003).

Let us now present more specific steps of the complete multi-PRI RV ambiguity mitigation scheme. We assume application to the lowest elevations, where range aliasing is most severe. First, a long-PRI scan is conducted to obtain signal-to-noise ratio (SNR) data from the entire spatial range of interest (just as is done in the "split cut" mode of the WSR-88D). Indexed radial beams are desired so that the long-PRI scan radials are aligned with subsequent scans. Then a multiblock-staggered (MBS) pulse train is transmitted in the subsequent scan, encoded with pseudorandom phase. The randomized phase enables selective coherence to any given trip, while signals from other trips are rendered incoherent. An MBS sequence consists of subsets of consecutive pulses at the same PRI. For example, a 3 x 16 MBS sequence is 16 pulses transmitted at PRI #1, another 16 at PRI #2, then 16 more at PRI #3. The reason for clustering pulses in blocks of the same PRI is because effective ground clutter filters (GCFs) can be designed for such sequences. In fact, an adaptive clutter filtering technique has been developed, which uses information gathered in the initial long-PRI scan (Cho and Chornoboy 2005); we refer the reader to that paper for further details.

For each dwell, to compute base data up to the range corresponding to the shortest PRI used we apply the first-trip-protection technique developed previously (Cho 2005). Between this range and the maximum range covered by the initial long-PRI scan we do the following. First, for each time increment l (associated with each pulse), loop through all gate indices. For each gate, find in the long-PRI data the signal power present in all the gates that would have aliased into this gate. The indices of the gates that would have aliased into gate k are given by

$$g_j = k + \mathrm{INT}\left(\frac{c}{2\Delta r} \sum_{i=1}^{j} T_{l-i} \right), \qquad (1)$$

where Δr is the range sampling interval, INT denotes conversion to nearest integer, and j (trip number – 1) goes up to the maximum integer that keeps g_j within the number of range gates in the long-PRI data. If the strongest signal power in gates g_j (denote by gate g_{MAX}) is stronger than the sum of signal powers at all other gates g_j and gate k, then the in-phase and quadrature (I&Q) complex sample of the MBS time series from gate k is stored for later processing in matrix **S**. The size of **S** is M x N, where $M = \mathrm{INT}[cT_L/(2\Delta r)] - g_{7MIN}$, T_L is the PRI of the long-PRI scan, $g_{7MIN} = \mathrm{INT}[cT_{MIN}/(2\Delta r)]$, T_{MIN} is the shortest PRI of the MBS sequence, and N is the number of pulses in the dwell. The indices for **S** in which the I&Q sample from gate k and pulse l is stored are given by l for the column index and $g_{MAX} - g_{7MIN}$ for the

row index. An important additional note is that before the I&Q sample is stored, it must be phase-cohered to the correct corresponding trip.

The previous loop over all gates uncovered the out-of-trip signals that were stronger than the first-trip signal for each pulse and stored the corresponding I&Q signal in the proper unfolded gate. Now we need to take care of the transition region gates where the available number of time samples is less than N, i.e., for ranges greater than the minimum r_a but less than or equal to the maximum r_a. For each time index l, loop over gates $g_{7MIN} + 1$ to INT$[cT_l/(2\Delta r)]$. If the signal power at gate k is greater than the sum of the out-of-trip signals in the long-PRI data, where the summation is carried out over gates given by (1), then the I&Q sample at gate k is stored in **S**. The indices for **S** in which the I&Q sample from gate k and pulse l is stored are given by l for the column index and $k - g_{7MIN}$ for the row index. These stored I&Q samples must be cohered to the first trip.

We now have in **S** all the available range-dealiased I&Q samples phase-cohered to the correct trips. Many elements of **S** are expected to be empty, since only the strongest-trip signals could be recovered for each pulse. It is now a simple matter to process **S** row-by-row for base data estimation at each gate. Samples from every PRI subset are processed using the pulse-pair algorithm. PRI subsets with no pairs available are thrown out. Median values are taken for reflectivity, velocity, and spectral width over the results from the PRI subsets. Velocity dealiasing using the clustering method (Trunk and Brockett 1993) is performed if two or more sets of PRIs produced estimates. The results are assigned to the proper gate given by the row index of **S** added to g_{7MIN}.

An additional complication to range dealiasing is the GCF. Applying a GCF coherently across all PRI pulse sets convolves information from different pulses and destroys the independence of range aliasing between PRI sets. In other words, even if only one PRI set is contaminated by an overlaid signal, application of the GCF will mix some of this unwanted signal into the time series of all the other PRI sets. Therefore, the GCF should only be applied when absolutely necessary. The procedure for minimizing GCF use is outlined by Cho (2005). If GCF is used on a gate, then range dealiasing is not attempted on that gate. Other relevant topics such as PRI set selection, velocity dealiasing, and false dealias correction are also discussed in that paper.

3. RESULTS USING SIMULATED WEATHER RADAR DATA

We now test the range-dealiasing procedure with simulated I&Q weather radar data for 360° scans. Within a range-azimuth space of 460 km x 360°, at 0.25-km and 1° resolution, reflectivity, velocity, and Doppler spectral width were specified for each cell. This specification was carried out through the definition of a background (constant for all space) plus any number of compact "patches." The patches were meant to mimic, in a crude way, storm cells and wind-field anomalies. These weather patches were specified as 2D Gaussians, so that their location, size, and shape were determined by the mean and standard deviation in the two dimensions. Cut-off boundaries were also defined so that computation for each patch would not have to be carried out over the entire domain. The velocity and spectral width of a patch were constant, except for a special type designed to look like a microburst, in which the velocity field was perturbed as a symmetric radial divergence with the perturbation magnitude decaying as a cosine from 0 to 90° with distance. Then for each range-azimuth cell, the resulting signal strengths and radial velocities (from the background and any patches) were computed, corresponding Doppler velocity spectra were generated and sampled with the PRI sequence using the standard technique (Zrnić, 1975) modified for nonuniform time sampling, and the resulting time-domain series summed together if needed. For short PRIs, out-of-trip signals were added to the first-trip signal using the appropriate phase multiplier associated with the pulse phase code. (For our study, we used a pseudorandom code.) Finally, white noise was added to simulate receiver noise. The radar wavelength was set to 10.5 cm.

Figure 2 shows the input reflectivity field for an example simulated scan. The background ("clear air") is set to a constant 0 dBZ with a spectral width of 2 m s^{-1}. The inner (dashed) circle shows the unambiguous range limit corresponding to the shortest PRI (987 μs) in the MBS sequence that will be used here. The outer (solid) circle indicates the unambiguous range limit corresponding to the longest PRI (1533 μs) in the MBS sequence. So this example will provide up to three trips for the shortest PRI subset and two trips for the longest PRI subset to cover the full 460-km range.

The patch to the north at close range is a "microburst" with a divergent velocity perturbation. There is also a patch further to the north that is out of first-trip range for all PRI subsets in the MBS sequence. Since these two patches line up along the same radials and their signals will be overlaid on top of each other at certain gates and pulses, they will provide a test of how well the range-dealiasing algorithm can separate them. Similarly, the two eastern patches line up in radial in different trips, but here the close-range patch is spatially extensive in the radial direction, so we would expect range dealiasing to be problematic. The southern patches are also aligned in radial, but the first-trip patch is narrow in radial extent, so range dealiasing with multi-PRI processing should be successful. For a single-PRI scan such that the distant southern patch folds on top of the nearby southern patch, this is a case where recovery of the outer patch by phase-code processing is expected to fail, because the peak overlay power ratio is 40 dB and the spectral width of the inner patch is wide (6 m s^{-1}) (Sachidananda and Zrnić 1999). Recovery of the western patches should encounter no interference from the weak first-trip background signal. The spectral width of all patches was set to 4 m s^{-1} except for the first-trip southern patch.

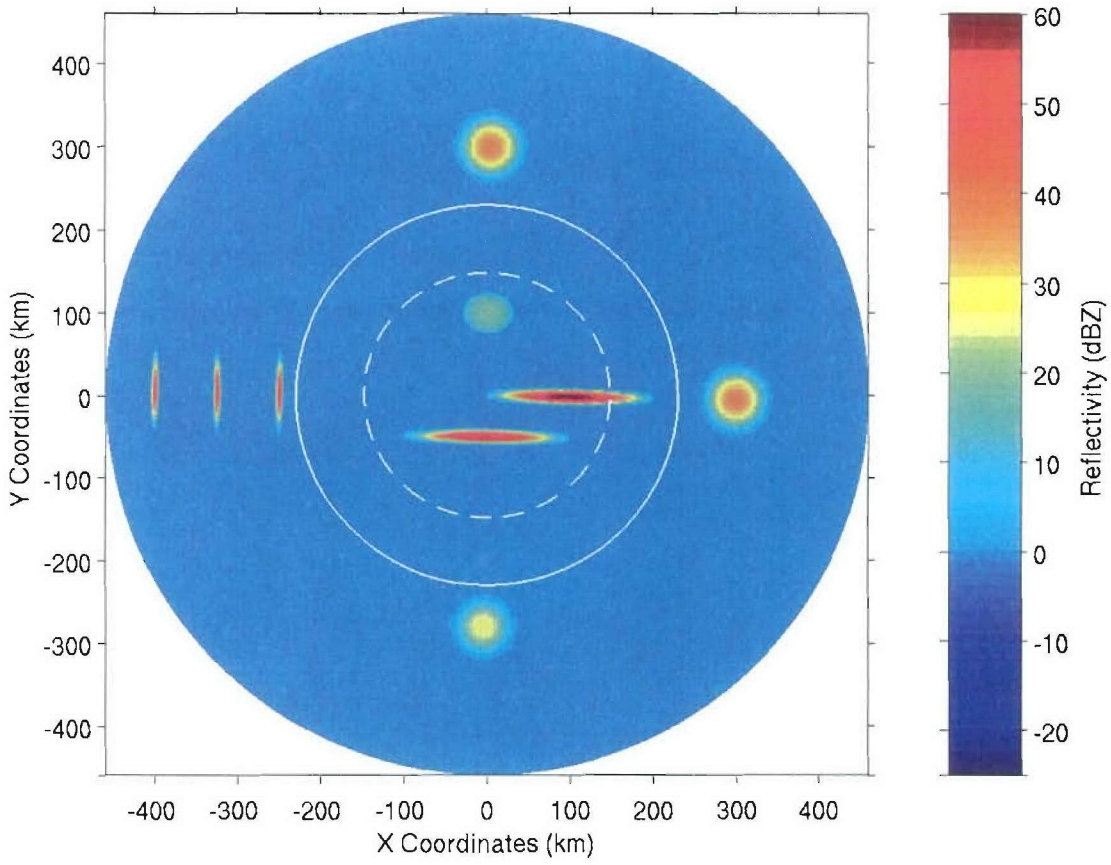

Figure 2. Reflectivity field input to simulated weather radar data. The inner (dashed) circle shows the unambiguous range limit corresponding to the shortest PRI (987 μs) in the MBS sequence. The outer (solid) circle indicates the unambiguous range limit corresponding to the longest PRI (1533 μs) in the MBS sequence.

Figure 3 shows the equivalent SNR plot. Radar parameters for the WSR-88D were used. Note that the background SNR approaches 0 dB by the time the range reaches the inner (dashed) circle, so the estimation of background velocity is expected to be challenging in the transition region between the inner and outer rings. Beyond the outer ring, estimates of the background quantities will not be possible.

Figure 4 shows the input velocity field. The maximum v_a of the PRI sets we will use in the example to follow is only 26.6 m s^{-1}, so velocity dealiasing will be needed to correctly recover greater velocity magnitudes.

I&Q data for the long-PRI scan were produced with a sampling period of 3066 μs and 18 pulses per 1° dwell. This scan was then processed with the standard pulse-pair algorithm for signal power and spectral width estimates. These estimates provided input to the subsequent multi-PRI signal processing.

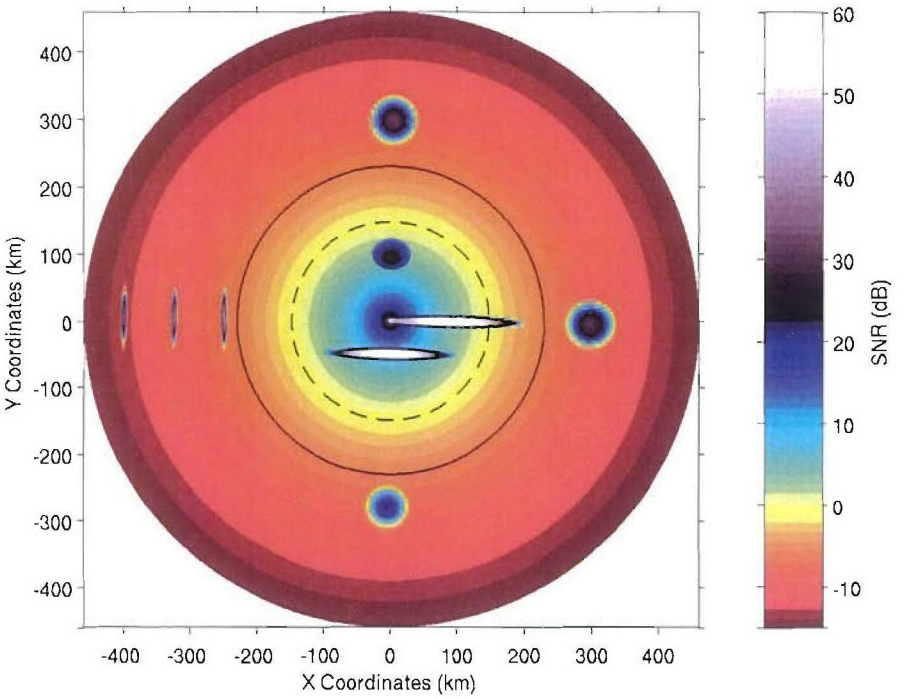

Figure 3. SNR field input to simulated weather radar data.

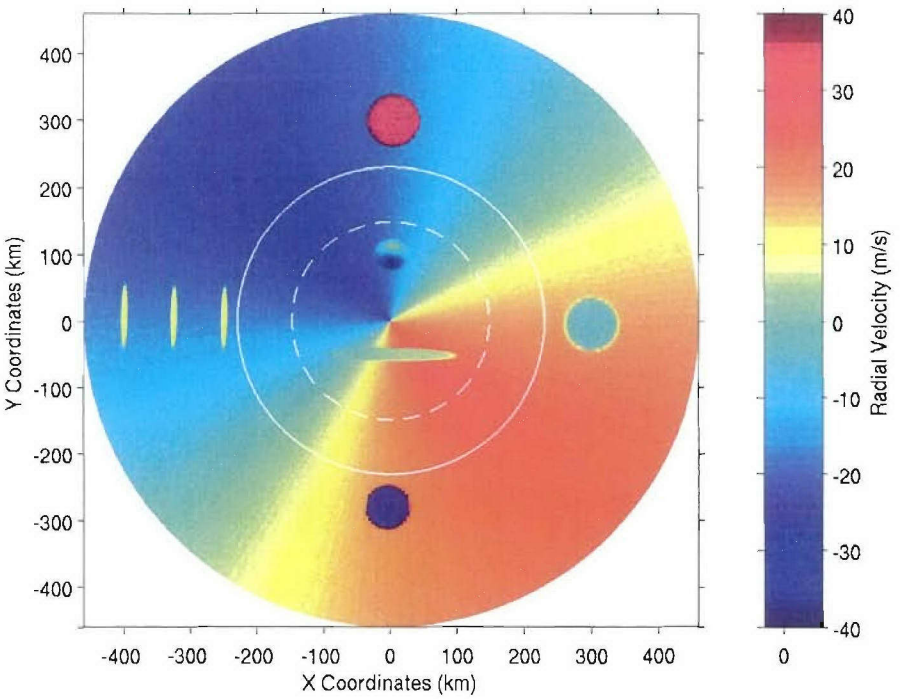

Figure 4. Radial velocity field input to simulated weather radar data.

Figure 5 shows reflectivity estimates computed by our range-dealiasing algorithm. The MBS sequence used was 4 x 11 with PRIs of 987, 1169, 1351, and 1533 μs. These values correspond to unambiguous ranges of 148, 175, 203, and 230 km, and Nyquist velocities of 26.6, 22.5, 19.4, and 17.1 m s^{-1}. For both the long-PRI and MBS scans, the number of pulses per 1° dwell corresponds to an antenna rotation rate of 18° s^{-1}. Both out-of-trip range reconstruction and first-trip protection for reflectivity work quite well except for the far eastern patch. As expected, the radially elongated patch at closer range has caused the central portion of the far eastern patch to be obscured. There is also some loss discernible at the edges of the far northern patch due to interference from the close-range northern patch.

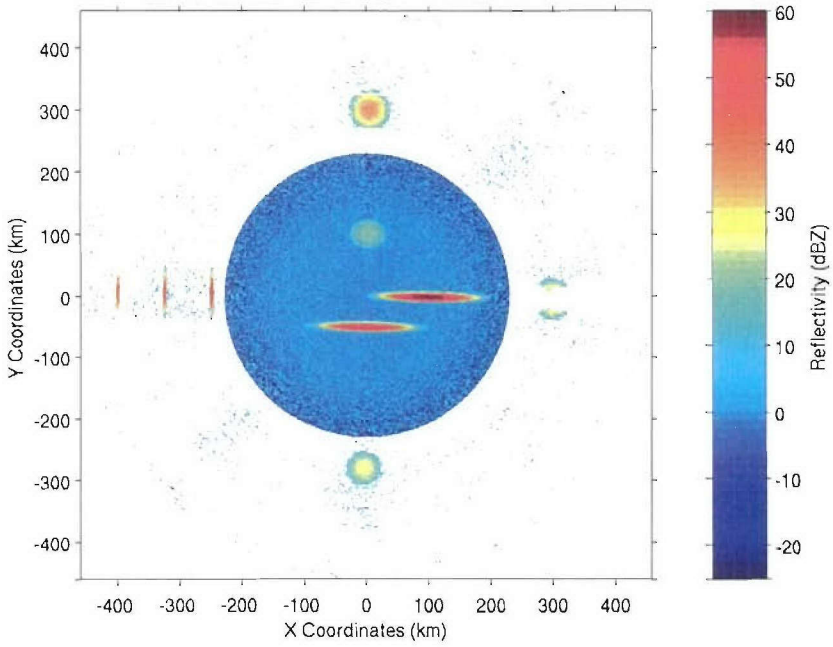

Figure 5. Reflectivity estimated from processed MBS signal. White regions indicate no data recovery.

Figure 6 shows the estimated radial velocity field. One can see the degradation of the estimate quality with increasing radial distance as the SNR decreases. There is even more degradation as the transition zone is entered and the number of available PRI subsets in the first-trip gates decreases. Then, as the number of PRIs goes from two to one, there is a sudden transition in the velocity field. With only one PRI available to estimate the low-level background velocity, aliasing becomes dominant for speeds greater than about 17 m s^{-1}, which is the Nyquist velocity of the longest PRI. However, velocity estimates for speeds less than this value are of better quality than at immediately closer range. This transition occurs because when no attempt is made to dealias the velocity, false dealiasing cannot occur to corrupt the data. For any velocity dealiasing method, it is better not to apply it if one knows a priori that the velocity is not aliased. In any case, for operational use, data censoring would remove the low-SNR region data, including the non-dealiased velocities.

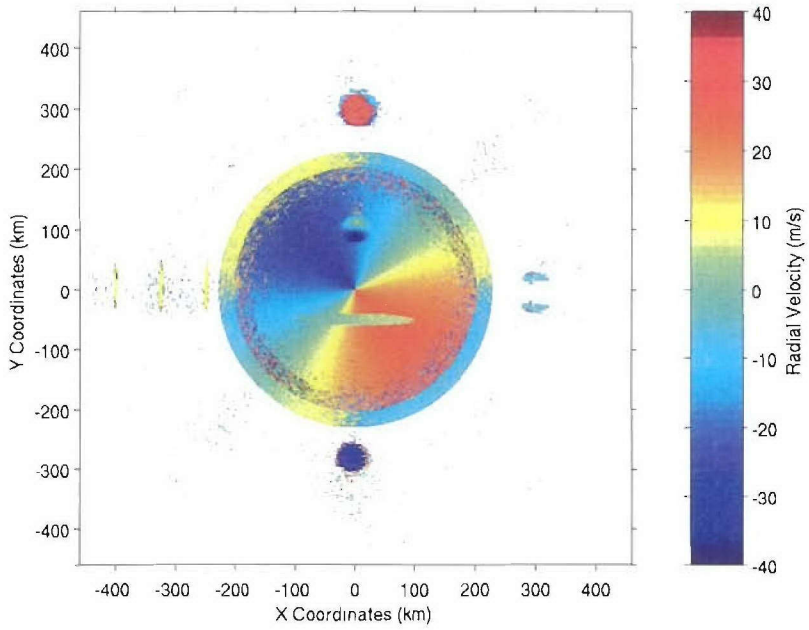

Figure 6. Radial velocity estimated from processed MBS signal. White regions indicate no data recovery.

For completeness we show the estimated spectral width field in Figure 7. We used lag 0 and lag 1 in the pulse-pair logarithm formula [Doviak and Zrnić 1993, their Eq. (6.27)]. This higher moment data field is also more sensitive to signal quality degradation. The estimate variance overall is higher than for velocity or reflectivity. One can see some hints of first-trip protection breakdown in the northern and southern radials (this is also slightly observable in the velocity field).

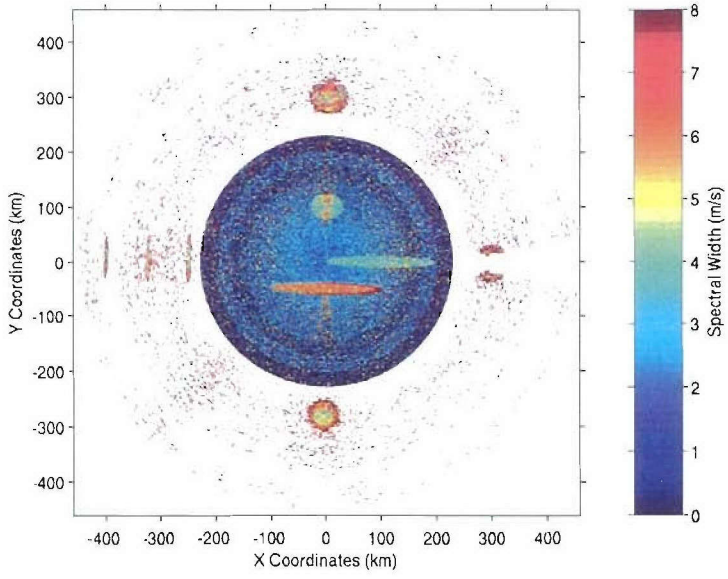

Figure 7. Spectral width estimated from processed MBS signal. White regions indicate no data recovery.

4. RESULTS USING REAL WEATHER RADAR DATA

Since we did not have access to multi-PRI I&Q data collected by a WSR-88D, we applied our algorithm to TDWR data. Collection of I&Q data was made possible with the installation of a prototype RDA at the FAA's Program Support Facility (PSF) TDWR in Oklahoma City. This prototype was designed by Lincoln Laboratory as part of an effort by the FAA to enhance supportability of their radar subsystems. The system control computer of the RDA houses a SIGMET RVP8, which provides the digital receiver, digital waveform shaping, and timing functions in three PCI cards each with several field programmable gate array (FPGA) chips. A combination of interrupt-driven software and FPGA code allows the system to change PRI and phase coding on a radial-by-radial basis, a key feature for the planned adaptive signal transmission and processing algorithms. For these tests, the I&Q data were merely recorded and were processed later off line.

The TDWR transmits a peak power of 250 kW. The antenna beam width is 0.55°, and the pulse length is 1.1 μs. The PSF TDWR operates at a frequency of 5.62 GHz. Although the operational system samples range at 150-m resolution, the first version of the RDA prototype used in this study sampled at 125-m resolution. (This has been updated to 150 m in the current version.) For further details on the TDWR see Michelson et al. (1990).

The data set presented here was collected on 17 March 2003 starting at 2040 UT, while convective storm cells were active in the vicinity. The scan elevation angle was 0.3° with an antenna rotation rate of 21.6° s^{-1}. Figure 8 shows the reflectivity field computed from the long-PRI (3.06 ms) scan for the full 460-km radius. Very strong scattering targets existed at many different ranges and azimuths, thus making this an interesting case for range dealiasing. In some azimuths there are multiple trips aliasing into the first trip. Further information about this particular case is presented by Cho (2005).

The range-dealiased MBS (518, 578, 638, 698, 758, 818, 878, 938 μs x 8 pulses each) reflectivity scan (Figure 9) displays an excellent likeness to the "truth" provided by Figure 8. There are still some areas of first-trip protection failure, but the reconstruction of the out-of-trip storm cells is very good. No significant weather patch at far range is missing. The far-range patches in the velocity plot (Figure 10) likewise appear to be an eminently reasonable reconstruction, but, of course, there is no "truth" available for comparison. We can only point out that the continuity of the field is consistent with physical reality. Figure 11 shows the spectral width field.

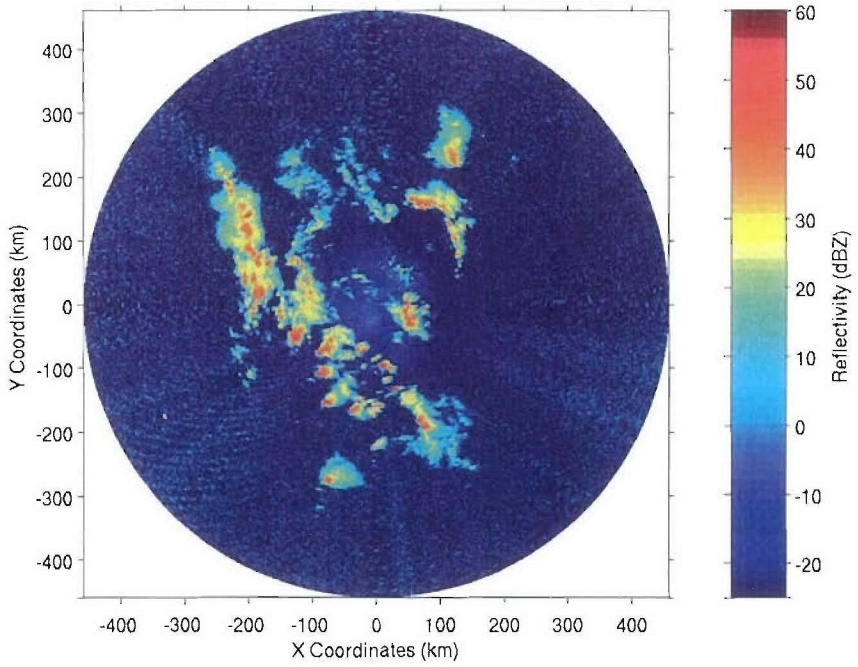

Figure 8. Reflectivity estimates from a long-PRI (3.06 ms) scan. The dataset was collected with the PSF TDWR in Oklahoma City on 17 Mar 2003 starting at 2040 UTC using the initial RDA prototype. The scan elevation angle was 0.3° with an antenna rotation rate 21.6° s^{-1}. An adaptive GCF and standard pulse-pair processing were used.

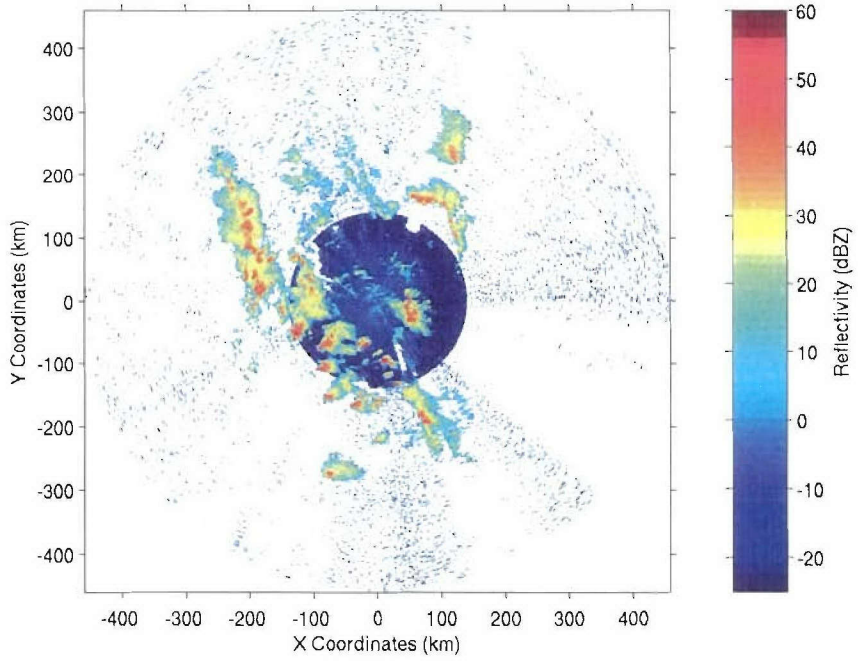

Figure 9. Reflectivity estimates from the MBS transmitted signal with range dealiasing. White areas indicate no data recovery.

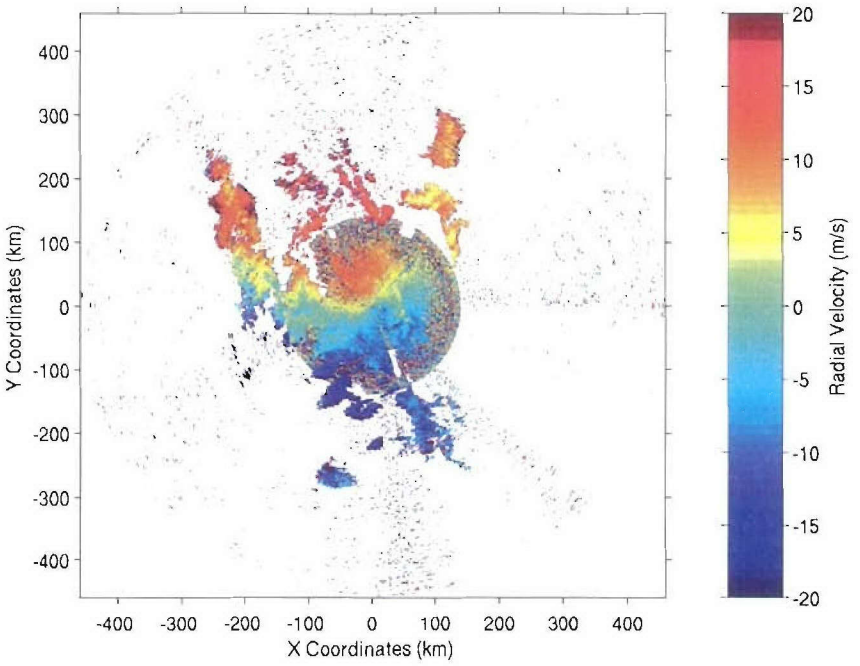

Figure 10. Radial velocity estimates from the MBS transmitted signal with range dealiasing. White regions indicate no data recovery.

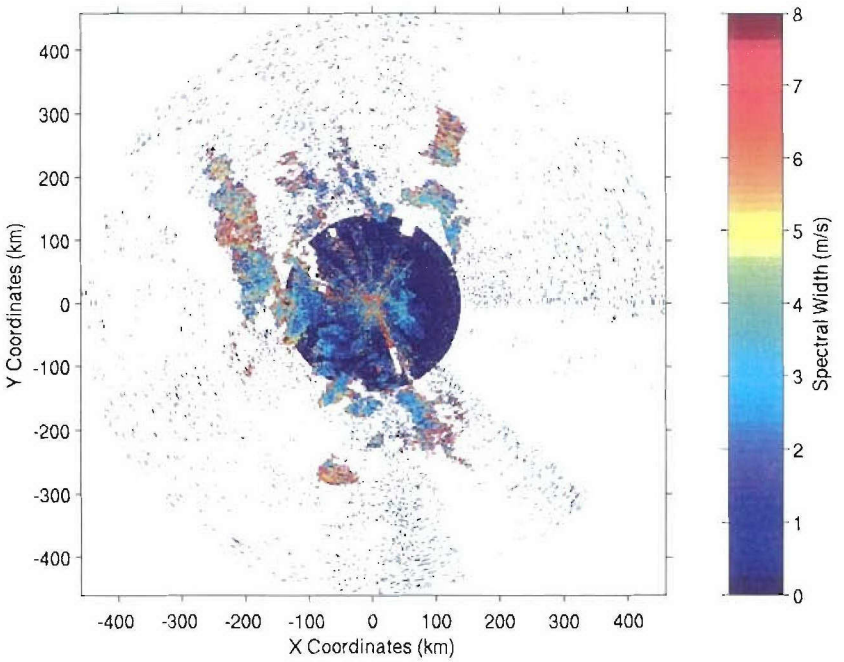

Figure 11. Spectral width estimates from the MBS transmitted signal with range dealiasing. White regions indicate no data recovery.

5. SUMMARY DISCUSSION

In this paper we extended the first-trip protection capabilities of the multi-PRI transmission and processing technique to include range-dealiased retrieval of out-of-trip weather radar data. Note that our scheme differs from the staggered-PRI unambiguous range extension method given by Sachidananda and Zrnić (2003), which only retrieves data within the first trip of the longer PRI. Example results using simulated weather radar data demonstrated the capabilities and limitations of the technique. Real data collected by a prototype TDWR RDA using multi-PRI transmission were also processed using this algorithm. The results showed excellent recovery of base data quantities at all ranges.

A drawback to using the multi-PRI technique is the difficulty in performing a full spectral analysis. However, band-limited analysis is available as an option for Doppler moment estimation (Weber and Chornoboy 1993; Chornoboy and Weber 1994) if spectral processing is deemed desirable.

In combination with the first-trip protection algorithm (Cho 2005) and adaptive GCF (Cho and Chornoboy 2005), multi-PRI unambiguous range extension is a viable technique for any weather radar. For the most effective RV ambiguity mitigation, it can be applied in the context of an adaptive signal transmission and processing scheme in which the optimal mode is selected on a dwell-by-dwell basis. In this scheme, a number of different MBS sequences could be available for selection, as well as constant-PRI phase-code processing. The latter mode can provide range dealiasing under conditions in which the multi-PRI technique fails, i.e., when the strong overlay has a long, continuous radial extent. We are planning to apply this adaptive technique to operational TDWR use in the future.

With phase-code processing using a single PRI, there is no instrinsic velocity dealiasing capability. This is not a problem if a short enough PRI can be employed to cover the required velocity measurement range. For example, with SZ phase-code processing, trip signal separation is not possible for a trip difference of four (e.g., between the first and fifth trips). Therefore, the minimum PRI that would be used if Doppler signal recovery out to 460 km is desired is 767 μs, which corresponds to r_a = 115 km and v_a = 34 m s^{-1} for the WSR-88D. If this unambiguous velocity range is insufficient, additional velocity dealiasing methods must be used, such as switching the PRI between two values after each dwell for interdwell velocity dealiasing. We plan to apply this technique in the enhanced TDWR RDA.

The multi-PRI approach, on the other hand, has a built-in velocity dealiasing capability that is flexible in meeting the required velocity measurement range. By using the unfolded velocity clustering method (Trunk and Brockett 1993), one can specify the maximum velocity range for which the dealiasing algorithm searches for the most likely velocity value. Unlike methods applying the Chinese Remainder Theorem, no particular PRI relationships are needed, and one can adjust the trade-off between velocity dealiasing error rate and maximum dealiased velocity range in a continuous, smooth manner (Cho 2005).

GLOSSARY

FAA	Federal Aviation Administration
GCF	Ground Clutter Filter
MBS	Multiblock-staggered
NEXRAD	Next Generation Weather Radar
ORDA	Open Radar Data Acquisition
PRI	Pulse Repetition Interval
PSF	Program Support Facility
RV	Range-velocity
SNR	signal-to-noise ratio
SQI	Signal Quality Index
TDWR	Terminal Doppler Weather Radar
WSR-88D	Weather Surveillance Radar-1988 Doppler

REFERENCES

Cho, J. Y. N., Evaluation of TDWR range-ambiguity mitigation techniques, Project Rep. ATC-310, MIT Lincoln Laboratory, Lexington, MA, 47 pp., 2003.

Cho, J. Y. N., Multi-PRI signal processing for the Terminal Doppler Weather Radar. Part II: Range-velocity ambiguity mitigation, *J. Atmos. Oceanic Technol.*, in press, 2005.

Cho, J. Y. N., and E. S. Chornoboy, Multi-PRI signal processing for the Terminal Doppler Weather Radar. Part I: Clutter filtering, *J. Atmos. Oceanic Technol.*, *22*, 575-582, 2005.

Cho, J. Y. N., G. R. Elkin, and N. G. Parker, Range-velocity ambiguity mitigation schemes for the enhanced Terminal Doppler Weather Radar, Preprints, *31st Conf. on Radar Meteorology*, Seattle, WA, Amer. Meteor. Soc., 463-466, 2003.

Chornoboy, E. S., and M. E. Weber, Variable-PRI processing for meteorological Doppler radars, Preprints, *1994 IEEE National Radar Conf.*, Atlanta, GA, 85-90, 1994.

Doviak, R. J., and D. S. Zrnić, *Doppler Radar and Weather Observations*, Academic Press, 562 pp., 1993.

Michelson, M., W. W. Shrader, and J. G. Wieler, Terminal Doppler Weather Radar, *Microwave J.*, *33*, 139-148, 1990.

Sachidananda, M., and D. S. Zrnić, Systematic phase codes for resolving range overlaid signals in a Doppler weather radar, *J. Atmos. Oceanic Technol.*, *16*, 1351-1363, 1999.

Sachidananda, M., and D. S. Zrnić, An improved clutter filtering and spectral moment estimation algorithm for staggered PRT sequences, *J. Atmos. Oceanic Technol.*, *19*, 2009-2019, 2002.

Sachidananda, M., and D. S. Zrnić, Unambiguous range extension by overlay resolution in staggered PRT technique, *J. Atmos. Oceanic Technol.*, *20*, 673-684, 2003.

Siggia, A., Processing phase coded radar signals with adaptive digital filters, Preprints, *21st Int. Conf. on Radar Meteorology*, Edmonton, AB, Canada, Amer. Meteor. Soc., 167-172, 1983.

Trunk, G., and S. Brockett, Range and velocity ambiguity reduction, Preprints, *1993 IEEE National Radar Conf.*, Lynnfield, MA, 146-149, 1993.

Weber, M. E., and E. S. Chornoboy, Coherent processing across multi-PRI waveforms, Preprints, *26th Int. Conf. on Radar Meteorology*, Norman, OK, Amer. Meteor. Soc., 232-234, 1993.

Zrnić, D. S., Simulation of weatherlike Doppler spectra and signals, *J. Appl. Meteorol.*, *14*, 619-620, 1975.